The Cryosphere Discuss., doi:10.5194/tc-2016-133, 2016
Manuscript under review for journal The Cryosphere
Published: 21 July 2016

The Cryosphere Discussions

Circumpolar polynya regions and ice production in the Arctic: Results from MODIS thermal infrared imagery for 2002/2003 to 2014/2015 with a regional focus on the Laptev Sea

Andreas Preußer[1], Günther Heinemann[1], Sascha Willmes[1], and Stephan Paul[2]

[1]Department of Environmental Meteorology, Fac. of Regional and Environmental Sciences, University of Trier, Behringstr. 21, Trier, D-54296, Germany.
[2]Alfred Wegener Institute, Helmholtz Centre for Polar and Marine Research, Am Handelshafen 12, 27570 Bremerhaven, Germany.

Correspondence to: Andreas Preußer (preusser@uni-trier.de)

Abstract. High-resolution MODIS thermal infrared satellite data are used to infer spatial and temporal characteristics of 16 prominent coastal polynya regions over the entire Arctic basin. Thin-ice thickness distributions (≤ 20 cm) are calculated from MODIS ice-surface temperatures, combined with ECMWF ERA-Interim atmospheric reanalysis data in an energy balance model for 13 winter-seasons (2002/2003 to 2014/2015; November to March). From all available swath-data, (quasi-) daily thin-ice thickness composites are computed in order to derive quantities such as polynya area and total thermodynamic (i.e. potential) ice production. A gap-filling approach is applied to account for cloud and data gaps in the MODIS composites. All polynya regions combined cover an average thin-ice area (POLA) of 184.3 ± 35.6 x10^3km^2 in winter. This allows for an average total wintertime accumulated ice production of about 1444 ± 258 km^3, whereby the Kara Sea region and the North Water polynya (both 19%) as well as scattered smaller polynyas in the Canadian Arctic Archipelago (all combined 15%) are the main contributors. Other well-known sites of polynya formation (Laptev Sea, Chukchi Sea) show smaller contributions and range between 2 and 7%. Compared to an earlier study on pan-Arctic polynya characteristics that utilized lower resolution passive microwave remote sensing data, our estimates are about 22% larger on average. This partly originates from the use of high-resolution MODIS data, which increases the capability to resolve small scale (> 2km) thin-ice features such as large leads. Despite the short record of 13 winter-seasons, positive trends in ice production are detected for several regions of the eastern Arctic (most significant in the Laptev Sea region with an increase of 6.8 km^3/yr) and the North Water polynya, while other polynyas in the western Arctic show a more pronounced variability with varying trends. We emphasize the role of the Laptev Sea polynyas as being a major influence on Transpolar Drift characteristics through a distinct relation between increasing ice production and ice area export. Overall, our study contains the most accurate characterization of circumpolar polynya dynamics and ice production to date which should be valuable for future modeling efforts on atmosphere- sea ice - ocean interactions in the Arctic.

The Cryosphere Discuss., doi:10.5194/tc-2016-133, 2016
Manuscript under review for journal The Cryosphere
Published: 21 July 2016

The Cryosphere
Discussions
Open Access

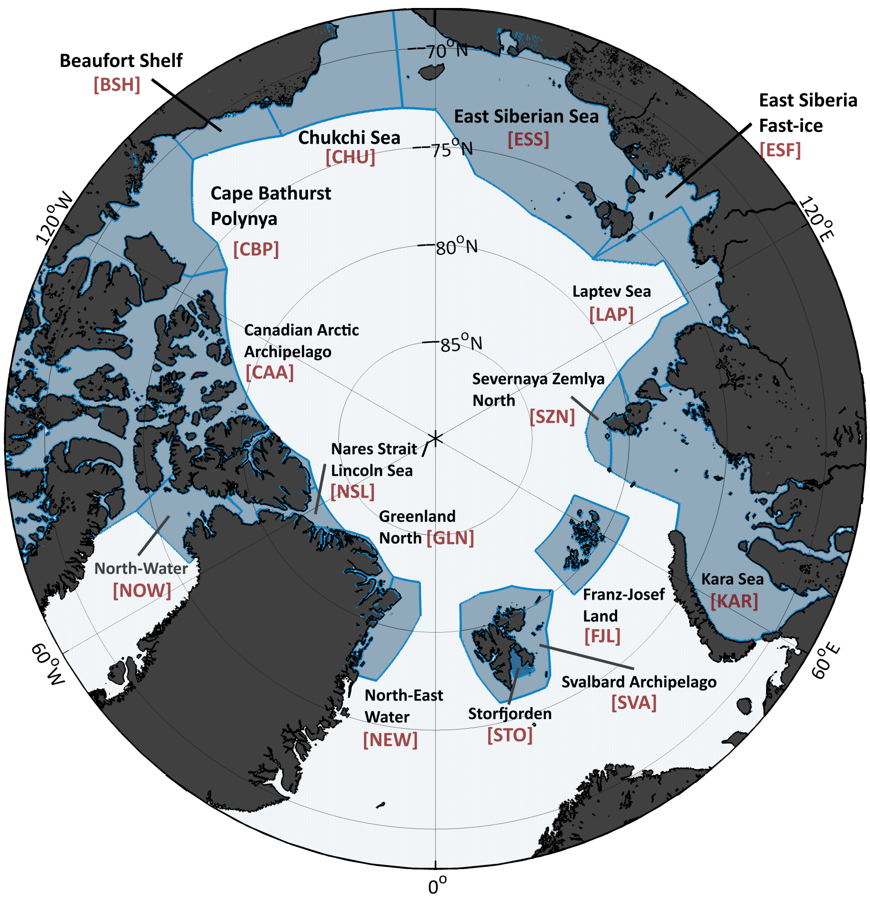

Figure 1. Map of all investigated areas of interest located in the Arctic, north of 68° N. The applied polynya masks are marked in blue, enclosing the typical location of each polynya in wintertime.

1 Introduction

The sea ice cover in the Arctic is subject to continuous changes through a variety of thermodynamic and dynamic processes, which are driven by atmosphere and ocean dynamics. Large areas of open water and thin ice (i.e. polynyas and leads) are characteristic features in this ice scape with a huge influence on local physical, biological and chemical processes at the interface between the atmosphere and the ocean (Barber and Massom, 2007).

Especially during wintertime, the presence of open water and thin ice leads to increased ocean to atmosphere heat fluxes, thereby allowing for new ice production and brine release as well as generally strong modifications of both the atmospheric boundary layer and upper ocean layers (Ebner et al., 2011; Gutjahr et al., 2016). Hence, an accurate assessment of wintertime sea-ice production in the Arctic is of vital interest for the understanding of Arctic sea-ice dynamics, the annual sea ice mass balance and, in general, for the verification of climate and ocean models. In case of the Arctic, it is widely considered that the

The Cryosphere Discuss., doi:10.5194/tc-2016-133, 2016
Manuscript under review for journal The Cryosphere
Published: 21 July 2016

main mechanism for polynya and lead openings are divergent ice motions caused by wind-induced stress (Smith et al., 1990). Therefore, most Arctic polynyas can be found adjacent to or in proximity of a fixed obstacle such as the coastline, attached land-fast ice or ice bridges under offshore-wind conditions (Williams et al., 2007). While the time of formation, the duration and the spatial extent of a polynya can be highly variable from year to year, their location of formation is generally rather stable (Morales-Maqueda et al., 2004). Leads are, in contrast, by far more variable both in space and time (Willmes and Heinemann, 2016). A regular monitoring of these open water and thin-ice areas with a high spatial accuracy is therefore a crucial step to be able to detect long-term changes, potential linkages and feedbacks to other environmental compartments as well as spatial and temporal patterns.

Based on the inventory of Barber and Massom (2007), we here define a total of 16 individual polynya regions in the Arctic north of 68° N (Fig.1). Some of these areas are designed to match reference areas in previous studies (e.g. Kern, 2008). The areal extent, i.e. the total ocean area, of each sub-region is depicted in Table 1. The vast majority of polynyas of our study is located around the Arctic shelf areas, with the largest fraction in the Siberian shelf region (East Siberian Sea (ESS), Laptev Sea (LAP), Severnaya Zemlya North (SZN), Kara Sea (KAR)). Other well-known sites of polynya formation are the North Water (NOW) Polynya in northern Baffin Bay, several other frequently appearing thin-ice zones around northern Greenland (Nares Strait / Lincoln Sea (NSL), Greenland North (GLN), North-East Water (NEW) polynya), the Storfjorden (STO) polynya in the Svalbard Archipelago (SVA) and a number of smaller polynya locations around Franz-Josef Land (FJL), the Canadian Arctic Archipelago (CAA) as well as the Beaufort (BSH and CBP) and Chukchi (CHU) Seas. The marginal ice zone (MIZ) in Fram Strait and west of Novaya Zemlya is excluded in our investigations due to a variety of potential ambiguities originating from ocean heat fluxes and a high interannual variability of the MIZ in terms of location and extent.

Pan-Arctic estimations of daily thin-ice thicknesses and ice production in polynyas were previously published by Tamura and Ohshima (2011) and Iwamoto et al. (2014), who both presented newly developed empirical thin-ice algorithms. Therein, commonly used passive microwave remote sensing data from the Special Sensor Microwave / Imager (SSM/I) and Advanced Microwave Scanning Radiometer - EOS (AMSR-E) satellite sensors is related to reference thin-ice thicknesses from Advanced Very High Resolution Radiometer (AVHRR) and Moderate Resolution Imaging Spectroradiometer (MODIS) thermal infrared data, based on a characteristic inverse relationship between the surface brine volume fraction and the thickness of sea ice (Iwamoto et al., 2014). In both studies, the advantages of passive microwave systems (complete daily coverage in the Arctic, almost no influence of clouds) come at the cost of quite coarse spatial resolutions (6.25 - 25 km) which strongly limit the ability to resolve small and/or narrow thin-ice areas in close proximity to coastlines or along fast-ice edges (Preußer et al., 2015a).

According to Willmes et al. (2011), a retrieval of long-term ice production is challenging for several reasons. First, the derivation of polynya area needs to be addressed with spatial and temporal resolutions, that are sufficient to capture the seasonal and regional dynamics of polynya events (Winsor and Björk, 2000; Morales-Maqueda et al., 2004; Tamura et al., 2008; Willmes et al., 2010). Second, the heat loss over the polynya has to be calculated, which requires detailed information about the fraction of open water, the ice thickness and its distribution within the polynya.

In order to address those challenges, the prime focus of this study is aimed towards the derivation of (quasi-) daily spatial thin-ice thickness distributions, which allows for a pan-Arctic retrieval of associated quantities like polynya area and thermo-

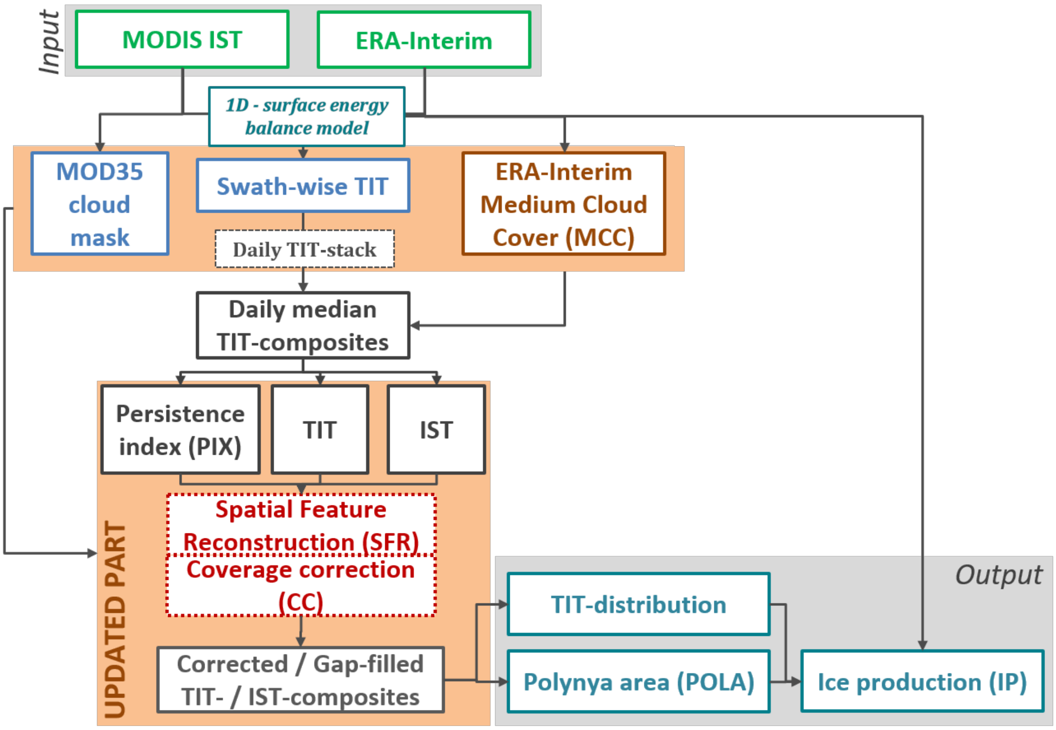

Figure 2. Schematic overview on the current version of the MODIS thin-ice thickness (TIT) retrieval scheme, based on Paul et al. (2015b) and Preußer et al. (2015a). The most recent updates are highlighted in orange and are mainly aimed towards an additional cloud-cover treatment. Besides indicated abbreviations, 'IST' denotes to ice surface temperature.

dynamic ice production. We make use of a high-resolution and long-term record of thermal-infrared data from MODIS, as measured ice-surface temperatures can be combined with atmospheric reanalysis data in a 1-D energy balance model (Adams et al., 2013) to obtain ice thicknesses up to 50 cm (Sect. 3.1). Based on these daily distributions and taking into account a necessary compensation for inherent cloud- and data gaps (Sect. 3.2), the amount of new sea-ice formation can be determined (Sect. 3.3). In Sect. 4, our achieved results will be presented and discussed, before closing this paper with final conclusions and prospects for further investigations. In recent studies using the same methodology based on MODIS data we focused on the NOW polynya (Preußer et al., 2015a) and the Storfjorden polynya (Preußer et al., 2015b). In the present study we have a strong focus on the Laptev Sea region, which is a central component of the transpolar drift system and showed significant changes in the last decade.

2 Data

2.1 MODIS ice-surface temperatures

The MOD/MYD29 Collection 5 sea-ice product (Hall et al., 2004; Riggs et al., 2006) is used to derive thin-ice thickness (TIT) from MODIS satellite data. It features swath data of ice-surface temperatures (ISTs) from both MODIS instruments on board the Terra and Aqua polar-orbiting satellite platforms. All swath data offer a spatial resolution of 1x1 km^2 at nadir and include a basic cloud-screening procedure using the MODIS cloud mask (MOD35; Ackerman et al. (2010)). In general, the accuracy of the MOD/MYD29 ISTs is given with 1–3 K (Hall et al., 2004). All IST swaths covering the Arctic Ocean and adjacent seas were extracted using meta data information for each MODIS swath. Subsequently, single swaths are mapped onto a common equirectangular (reference-) grid covering all areas north of 68° N , with the output resolution set at 2 km. For our analysis between 2002/2003 and 2014/2015 (November to March), we used a total of 143,000 MODIS swaths for the complete Arctic domain, averaging at 73 scenes per day.

2.2 ERA-Interim atmospheric reanalysis data

In order to provide the necessary atmospheric input for the applied surface energy balance model, the following variables from the European Center for Medium-Range Weather Forecasts (ECMWF) ERA-Interim reanalysis product (Dee et al., 2011) are used: 2m-temperature, 2m-dew point temperature, 10m-wind speed and mean sea-level pressure. As the use of the MOD35 cloud mask during nighttime often inhibits misclassifications and ambiguities from undetected clouds and sea smoke, we additionally utilize ERA-Interim medium cloud cover (MCC) information. The study of Liu and Key (2014) demonstrated that the ERA-Interim MCC fields correspond closely to the MODIS derived cloud patterns throughout the seasons and can therefore be used as an additional quality control during the TIT retrieval. The temporal resolution of all variables is 6 h, so that each single MODIS swath can be linked to the closest time step of the atmospheric fields from ERA-Interim for the calculation of thin-ice thickness. The data set is provided by ECMWF at a spatial resolution of 0.75° (approx. 80 km). All ERA-Interim data fields are linearly interpolated and projected on the common reference grid in order to match the higher spatial resolution of MODIS data.

3 Methodology

3.1 MODIS thin-ice thickness retrieval using a surface energy balance model

We derive daily TIT distributions up to 50 cm by using an approach that follows the work of Yu and Rothrock (1996), Yu and Lindsay (2003) and Drucker et al. (2003). The core of this approach is an one-dimensional energy balance model, in which ice surface temperature (IST) and the thin-ice thickness are related to atmospheric radiation fluxes and turbulent heat fluxes. The original method of Yu and Rothrock (1996) was improved and modified by Willmes et al. (2010) and Adams et al. (2013), while the latest modifications of the algorithm are described in detail in Preußer et al. (2015b, a) and Paul et al. (2015b). A complete overview on the currently used data-processing chain is given in Fig. 2.

There are certain limitations and simplifications attached to this procedure to derive TIT. First, it is only applicable to clear sky conditions, as clouds and sea smoke would strongly alter the recorded IST (Riggs et al., 2006). Second, we only use nighttime scenes to avoid potential ambiguities from incident short-wave radiation (Yu and Lindsay, 2003; Adams et al., 2013). Furthermore, newly formed ice is assumed to be free of snow and the temperature profile between the surface (IST) and the lower boundary of the ice (constant; freezing point of sea water) is linear.

The study of Adams et al. (2013) presented a sensitivity analysis of the TIT retrieval, which revealed average uncertainties of $\pm$ 1.0 cm, $\pm$ 2.1 cm and $\pm$ 5.3 cm for TIT classes 0–5 cm, 5–10 cm and 10–20 cm, respectively. Between 20–50 cm, the uncertainty increases considerably. Therefore, we constrain our analysis accordingly as a thickness range of TIT ≤ 0.2 m is widely regarded as a threshold for polynya areas and for estimates of thermodynamic ice production in polynyas (Yu and Rothrock, 1996; Adams et al., 2013; Haid et al., 2015).

3.2 Calculation of daily TIT composites and correction of cloud- and data gaps

Because of the restriction to nighttime scenes, a less frequent IST coverage is present in the beginning (November) and at the end (March) of each winter-season. In order to increase the IST coverage for all considered areas (Fig. 1), we derive daily composites of IST and TIT from the total number of available MODIS swaths covering the Arctic domain on a given day (compare Sect. 2.1). Following the procedure described in Sect. 3.1, the TIT is first calculated from each single swath on its own. Subsequently, the daily median TIT per pixel is calculated and stored alongside its corresponding IST value and daily averaged energy-balance components.

As described in Sect. 2.2, we additionally make use of ERA-Interim MCC fields as an indicator for potential cloud-coverage during the generation of daily TIT composites. Previous studies showed that a threshold of 75 % cloud-cover in the MCC-fields is quite effective in identifying and filtering/removing potentially cloud-affected areas (Paul et al., 2015b; Preußer et al., 2015a). The combined MODIS and ERA-Interim cloud information allows for the assignment of four different quality-classes for each pixel in the daily composites: (1) confident clear-sky pixels (clear-sky MODIS and ERA-Interim), (2) mixed-covered pixels (ratio between clear-sky input swaths and the total number of input swaths per pixel), (3) definitive cloud-covered pixels (both in MODIS and ERA-Interim) and (4) completely uncovered pixels.

Paul et al. (2015b) introduced an additional cloud-cover check based on the daily persistence of each pixel that is classified as thin ice (TIT ≤ 0.2 m). Misclassified thin-ice detections (i.e. clouds) are generally associated with low persistence-values due to their more mobile nature and displacements on sub-daily time scales. In contrast, polynyas show a higher spatial and temporal persistence due to their distinct formation mechanisms (Sect. 1). Leads, however, may be discarded by this criteria, since they generally have a low persistence due to their short lifetime and sea-ice drift caused by wind, ocean currents and tides. Based on these simple but distinct relations, we use a pixel-wise persistence index (PIX), defined as the ratio between the total number of MODIS swaths that feature thin-ice and the total number of swaths that feature clear-sky conditions.

The Cryosphere Discuss., doi:10.5194/tc-2016-133, 2016
Manuscript under review for journal The Cryosphere
Published: 21 July 2016

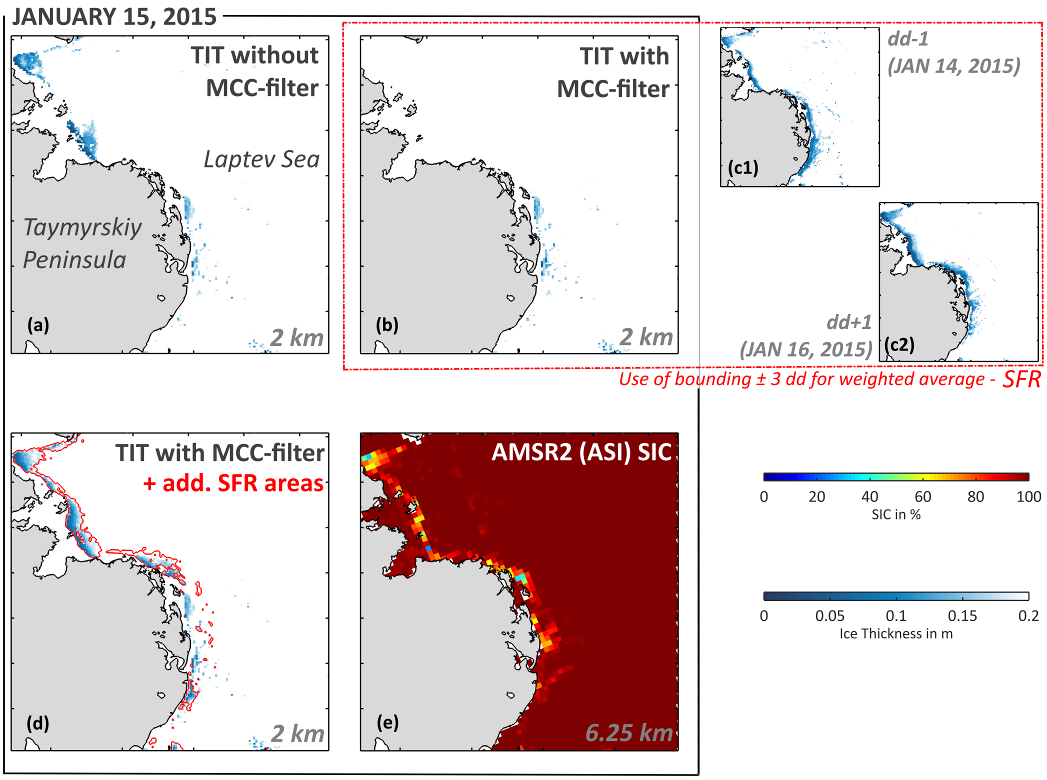

Figure 3. Different stages in the MODIS thin-ice thickness (TIT up to 0.2 m) processing chain for a single exemplary day (January 15, 2015). Sub-panels (a), (b), (c1/c2) and (d) all feature a subset (north-western Laptev Sea) from daily pan-Arctic TIT composites, with (a) showing the daily TIT without any cloud-treatment besides the MOD35 cloud mask and (b) the resulting TIT distribution after applying the ERA-Interim medium cloud cover (MCC) filter. Two bounding days with a better coverage of TIT are featured in panels (c1) and (c2) as a reference for the highest relative contribution in the spatial feature reconstruction (SFR) algorithm. The resulting spatial distribution of TIT after application of SFR is shown in panel (d), with new additional / reconstructed areas (up to 20 cm) marked in red. A comparison with Advanced Microwave Scanning Radiometer-2 (AMSR2) ASI sea-ice concentrations (Spreen et al. (2008); University of Bremen) from the same date is given in (e). The respective grid-resolution is given in the lower right corner of each sub-panel.

The Cryosphere Discuss., doi:10.5194/tc-2016-133, 2016
Manuscript under review for journal The Cryosphere
Published: 21 July 2016

All derived quality attributes (MCC-filter, cloud-cover information, PIX) are utilized in the Spatial Feature Reconstruction (SFR) algorithm (Paul et al., 2015a), which was recently successfully applied on a regional scale in both the Antarctic and Arctic to increase the information about otherwise cloud-covered areas (Paul et al., 2015b; Preußer et al., 2015a). The basic principle is that cloud-induced gaps in the daily TIT composites are compared with the TIT of the surrounding six days. In doing so, a probability of thin-ice occurrence is derived using a weighted composite of the surrounding days. The procedure is applied on all areas with identified low-quality data (low persistence, cloud-covered), so that indicated gaps can be filled with new information on potential thin-ice occurrences. For these areas, new TIT and IST values are pixel-wise allocated using a weighted average of the surrounding six days (Paul et al., 2015b; Preußer et al., 2015a). Table 1 gives an overview on the achieved IST and TIT coverage before and after application of the SFR algorithm. On a pan-Arctic level, the average (2002/2003 to 2014/2015) coverage is increased from around 0.76 (ccs and high-quality mcp) to 0.94 (including SFR areas), with certain regions performing better (e.g. CBP, LAP, NEW, SZN) and some other regions noticeably worse (CHU, GLN).

Case studies in the Brunt Ice Shelf region of Antarctica demonstrated the good performance of the algorithm by reproducing artificially cloud covered thin-ice areas with an average spatial correlation of 0.83 (Paul et al., 2015a). As an additional example from the Arctic (north-western Laptev Sea), Fig. 3 visualizes the basic principle of the SFR algorithm, together with a qualitative comparison of Advanced Microwave Scanning Radiometer 2 (AMSR2) sea-ice concentration (SIC) data (Spreen et al., 2008). As a first step, the MCC-filter eliminates potentially cloud-influenced areas which are in this case located north of the Taymyr Peninsula (Laptev Sea, Russia). One could argue that this filtering is a bit harsh, but we choose a more conservative threshold to minimize the risk of 'false' thin-ice pixels. Afterwards, the SFR algorithm is applied and a new gap-filled TIT composite (Fig. 3 (d)) is produced. In this particular example from January 15, 2015, the reconstructed TIT distribution compares well with locations of lower SIC from AMSR2 (Fig. 3 (e)) while maintaining the increased spatial detail at the same time. We conclude that the applied schemes to compensate and correct cloud-effects work reasonably well and allow for a fair comparison to other commonly used remote sensing approaches to infer polynya characteristics, with limitations regarding the reconstruction of leads.

3.3 Derivation of ice production and polynya area

Ice production rates are derived by assuming that the entire heat loss at the ice surface to the overlying atmosphere contributes to new ice formation (Tamura et al., 2007, 2008; Willmes et al., 2011). Components for the following equation (Eq. 1) can be taken from calculated and gap-filled daily MODIS composites.

$$\frac{\partial h}{\partial t} = \frac{-\bar{Q}_{ice}}{\rho_{ice} * L_f} \quad (1)$$

Therein, $\frac{\partial h}{\partial t}$ denotes to the ice production rate, $\bar{Q}_{ice}$ is the daily mean conductive heat flux through the ice, ρ_{ice} is the density of the ice ($\rho_{ice} = 910\ \mathrm{kg/m^3}$; Timco and Frederking (1996)) and L_f is the latent heat of fusion of sea ice ($L_f = 0.334\ \mathrm{MJ/kg}$; Tamura and Ohshima (2011)). Concerning L_f, Tamura and Ohshima (2011) noted that an accurate value for areas of high ice production is not known so far. Following the work of Martin (1981), Tamura and Ohshima (2011) argued that frazil ice

Table 1. Areal extents (i.e. total ocean area) of all applied polynya masks in km^2, together with the interannual average coverage (decimal cover fraction ranging from 0 to 1) before (COV2) and after (COV4) application of the Spatial Feature Reconstruction (SFR) for each polynya region from 2002/2003 to 2014/2015 (November to March). The abbreviation 'ccs' denotes to confident clear-sky coverage, while 'HQ mcp' are high-quality mixed-cover pixels where either MODIS or ERA-Interim medium cloud cover feature cloud signals in the daily composites. In addition, the average thin-ice thickness (TIT, in cm) inside each polynya region (for all TIT ≤ 0.2 m) is given together with its standard deviation. An overview on all applied predefined polynya masks is given in Fig. 1.

Region	*Total ocean area* ($10^3\mathrm{km}^2$)	*COV2* (ccs, HQ mcp)	*COV4* (ccs, HQ mcp, SFR)	*Avg. TIT* (cm)
Beaufort Shelf (BSH)	91.6	0.76 ± 0.03	0.97 ± 0.02	14.0 ± 0.5
Canadian Arctic Archipelago (CAA)	719.6	0.82 ± 0.03	0.96 ± 0.01	13.7 ± 0.2
Cape Bathurst (CBP)	311.6	0.81 ± 0.03	0.98 ± 0.01	14.1 ± 0.4
Chukchi Sea (CHU)	286.0	0.55 ± 0.04	0.79 ± 0.03	12.8 ± 0.4
East Siberian Fast-Ice (ESF)	110.1	0.77 ± 0.04	0.96 ± 0.01	14.3 ± 0.3
East Siberian Sea (ESS)	904.1	0.70 ± 0.03	0.92 ± 0.01	14.0 ± 0.3
Franz-Josef-Land (FJL)	140.1	0.79 ± 0.04	0.97 ± 0.02	11.7 ± 0.8
Greenland North (GLN)	33.8	0.67 ± 0.04	0.81 ± 0.04	16.3 ± 0.4
Kara Sea (KAR)	725.5	0.75 ± 0.04	0.95 ± 0.02	11.7 ± 1.1
Laptev Sea (LAP)	281.1	0.80 ± 0.03	0.98 ± 0.01	13.5 ± 0.5
North East Water (NEW)	112.0	0.81 ± 0.03	0.98 ± 0.01	13.7 ± 0.5
North Water (NOW)	110.1	0.85 ± 0.04	0.97 ± 0.01	11.5 ± 0.5
Nares Strait / Lincoln Sea (NSL)	55.5	0.83 ± 0.03	0.96 ± 0.01	13.6 ± 1.0
Storfjorden (STO)	11.7	0.75 ± 0.04	0.95 ± 0.03	9.2 ± 1.7
Svalbard Archipelago (SVA+STO)	204.3	0.68 ± 0.06	0.90 ± 0.04	7.2 ± 1.0
Severnaya Zemlya North (SZN)	65.3	0.80 ± 0.04	0.98 ± 0.01	13.5 ± 0.6
Total	4159.6	0.76 ± 0.04	0.94 ± 0.02	13.1 ± 0.6

consists of freshwater ice crystals enclosed with a thin saline layer and that frazil ice production rates are of similar magnitudes as freshwater ice production rates. Consequently, we also use fixed values for ρ_{ice} and L_f in order to ensure comparability with earlier studies focusing on sea-ice production in (Arctic) polynyas (e.g. Willmes et al., 2011; Tamura and Ohshima, 2011; Iwamoto et al., 2014). However, this simplification may introduce an additional error source in our estimates due to spatially and temporally varying conditions for ice formation. Note that the negative sign in Eq. 1 implies that the atmospheric heat flux is positive when the surface gains energy, and at the same time it assures that ice production only takes place when there is a net energy loss from the surface. According to the surface energy balance, the heat flux $\bar{Q}_{ice}$ is equal to the total atmospheric heat loss (sum of net radiation, turbulent latent and sensible heat flux). We do not consider an ocean heat flux, although it might potentially reduce thermodynamic ice growth in certain areas of the Chukchi Sea (Hirano et al., 2016), the Canadian Arctic Archipelago (Hannah et al., 2009) and northern Baffin Bay (Steffen, 1985). The volume ice production rate $\frac{\partial V}{\partial t}$ (*IP*) is calculated by multiplying $\frac{\partial h}{\partial t}$ with the areal extent of each pixel in the regarded region. Ice production rates are calculated for each pixel with a TIT ≤ 0.2 m and afterwards extrapolated to daily rates. However, it has to be noted that daily IP rates may inhibit a positive bias due to the exclusive use of both nighttime and clear-sky MODIS scenes. The former is mainly of concern during the late autumn / early spring period when polar night conditions are absent, while the latter circumstance is unavoidable throughout each winter when relying on optical remote sensing data.

The daily polynya area (POLA, in km^2) in each polynya mask (Fig. 1) is defined as the accumulated total area of all thin-ice pixels with a TIT ≤ 0.2 m. Remaining coverage gaps after the application of the SFR approach (e.g. prolonged periods of stable cloud cover, i.e. no coverage on more than 3 consecutive days) are handled by additionally applying an extrapolation approach (coverage-correction; CC) on calculated POLA and IP estimates, which yields daily values with an error-margin of 5 to 6% (Preußer et al., 2015b, a). If the daily coverage including the additional SFR areas (COV4) falls below 0.5, both daily POLA and IP inside the respective reference areas are linearly interpolated from bounding days.

4 Results and Discussion

4.1 Thin-ice dynamics, polynya area and thermodynamic ice production in the Arctic for 2002/2003–2014/2015

Interannual average values for TIT ≤ 0.2 m are listed in Table 1 for each polynya region. They range between 7.2 cm (SVA) and 16.3 cm (GLN), with an overall average of about 13.1 ± 0.6 cm. The underlying long-term time series of average wintertime TIT within each polynya reveal a tendency towards decreasing thin-ice thicknesses in almost every region (e.g. up to 2.5 cm per decade in the Kara Sea), with the only exceptions being the CAA, GLN and NEW.

Thin-ice frequencies of larger than 0.5 are found around the Canadian Arctic, first and foremost in the NOW-polynya and the eastern CAA (Fig. 4). More specifically, coastal areas around Devon Island and south-eastern Ellesmere Island (Hells Gate / Cardigan Strait) and larger areas at the eastern exits of Lancaster Sound and Jones Sound are well visible and have previously been related to tidal currents and slightly increased ocean heat fluxes (Hannah et al., 2009; Melling et al., 2015). Besides, elongated thin-ice areas along the Siberian shelf (Laptev and Kara Sea; frequencies around 0.05 to 0.35 each month) are well delineated. Locations of frequent thin-ice occurrences in the Kara Sea are in accordance with results from the study of Kern (2008). The northern Barents Sea, Franz-Josef-Land and the Svalbard archipelago / Storfjorden also feature quite high appearance rates of around 0.1 to 0.3. Contrary to earlier reports (Barber and Massom, 2007), the North-East Water (NEW) polynya in north-eastern Greenland (approx. 81° N, 13° W) neither shows any sign of disappearance, nor is it limited to the spring to late autumn period. With average frequencies of around 0.1 to 0.25 each month in winter, it has more likely to be categorized as a regularly forming polynya. Comparatively low frequencies below 0.15 (especially from January to March) are primarily found in the Beaufort and Chukchi Sea as well as in the East Siberian Sea. Vast fast-ice areas, e.g. along the Siberian coast, can be detected from monthly TIT frequencies, as these areas usually appear at fixed locations attached to the shore and TIT frequencies tend towards zero as the ice quickly thickens by congelation ice growth. Hence, our 13-year record of monthly TIT-occurrence rates offers the potential to further develop and optimize automatic methods for a regular Arctic-wide mapping of monthly fast-ice extents.

The Cryosphere Discuss., doi:10.5194/tc-2016-133, 2016
Manuscript under review for journal The Cryosphere
Published: 21 July 2016

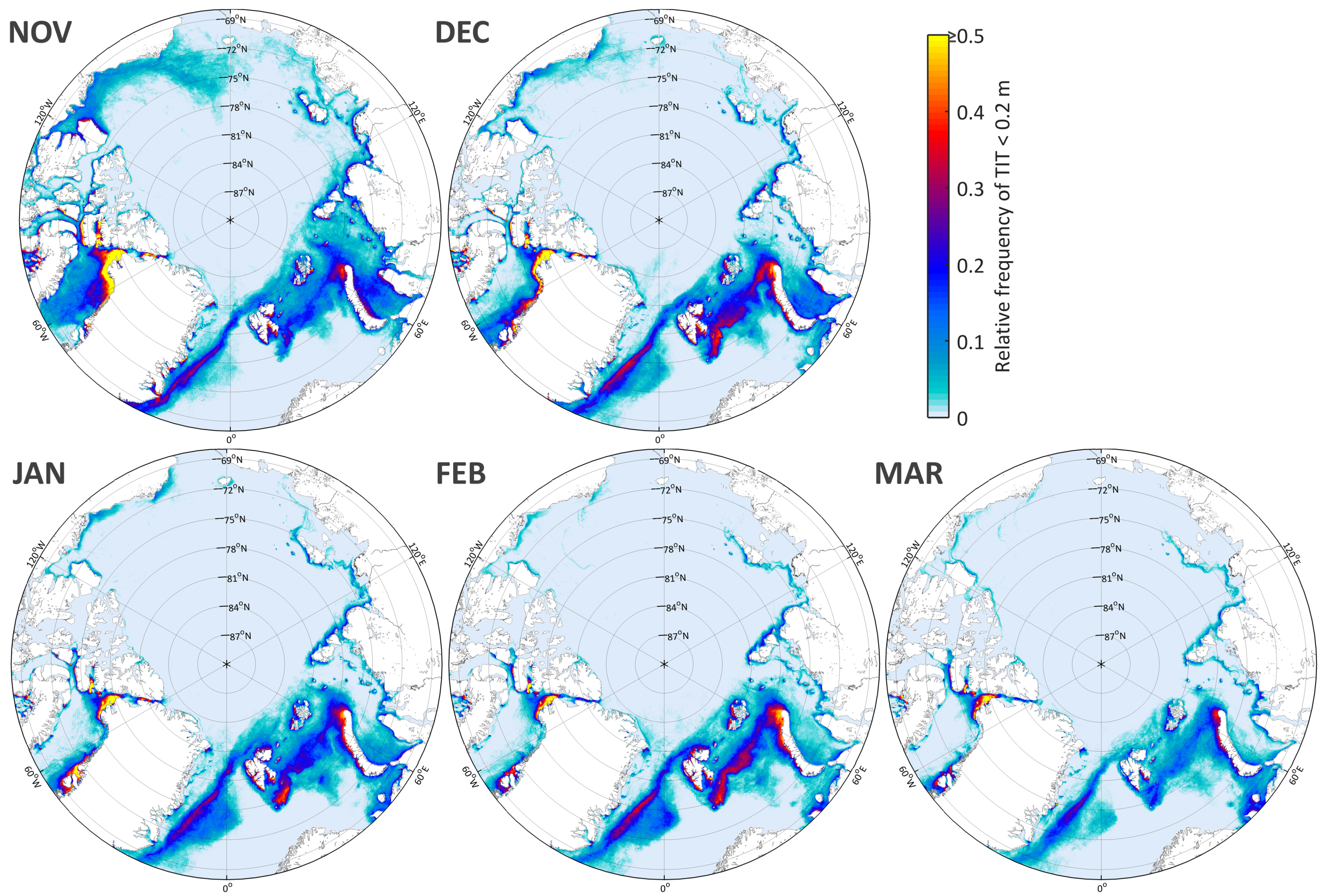

Figure 4. Average wintertime (November to March) frequencies of TIT ≤ 0.2 m in the Arctic between winters 2002/2003 and 2014/2015. Note that areas with high TIT frequencies in the marginal ice zone (MIZ) around Fram Strait and Barents Sea are excluded from further analysis due to potential ambiguities originating from ocean heat fluxes and a high interannual variability of the MIZ in terms of location and extent.

Table 2. Average accumulated ice production in km^3 per winter and average polynya area (in km^2) for each polynya region from 2002/2003 to 2014/2015 (November to March, with SFR cloud-cover correction). All values are derived from daily MODIS TIT composites after application of the predefined polynya masks (Fig. 1) Trends of IP and $POLA$ are additionally given, where underlined, bold and bold italic numbers denote statistical significance at the 90, 95 and 99 % level, respectively.

Region	*Acc.* IP (km^3)	*Trend* IP (km^3/yr)	$POLA$ (10^{3}km^2)	*Trend* $POLA$ (km^2/yr)
Beaufort Shelf (BSH)	23 ± 23	-0.5	2.7 ± 2.4	-12.8
Canadian Arctic Archipelago (CAA)	215 ± 43	5.4	24.9 ± 5.1	648.5
Cape Bathurst (CBP)	78 ± 54	1.0	10.4 ± 7.6	204.9
Chukchi Sea (CHU)	27 ± 16	-0.5	3.7 ± 2.2	-50.2
East Siberian Fast-Ice (ESF)	9 ± 5	**0.8**	1.1 ± 0.74	**109.5**
East Siberian Sea (ESS)	41 ± 13	1.5	5.7 ± 2.1	175.4
Franz-Josef-Land (FJL)	99 ± 41	5.6	12.9 ± 6.0	850.4
Greenland North (GLN)	5 ± 4	0.2	0.6 ± 0.5	27.8
Kara Sea (KAR)	277 ± 111	12.6	40.2 ± 15.8	1839.2
Laptev Sea (LAP)	96 ± 33	***6.8***	12.1 ± 4.2	***844.8***
North East Water (NEW)	22 ± 7	-0.4	2.8 ± 0.8	-37.1
North Water (NOW)	277 ± 67	6.0	30.3 ± 6.7	710.7
Nares Strait / Lincoln Sea (NSL)	39 ± 22	0.2	4.4 ± 2.3	4.0
Storfjorden (STO)	21 ± 6	**0.9**	3.3 ± 1.0	139.4
Svalbard Archipelago (SVA+STO)	214 ± 33	0.8	29.9 ± 4.9	487.5
Severnaya Zemlya North (SZN)	22 ± 11	***2.0***	2.6 ± 1.5	***263.0***
Total	1444 ± 258	**41.5**	184.3 ± 35.6	**6055.8**

Compared to the study of Willmes and Heinemann (2016), leads are only weakly visible in this long-term averages (frequencies below 0.05–0.1). In Fig. 4, leads are mainly located in the area of the Beaufort Sea and north of Greenland (shear zones). Further, they appear along the Transpolar Drift, a large-scale drift system where ice from the Siberian coastal regions is advected across the Arctic Ocean and through Fram Strait. Frequent lead occurrences in e.g. the East-Siberian Sea found by Willmes and Heinemann (2016) are not reflected in our study. In some regions, however, the influence of (shelf-) bathymetry and associated ocean currents on the spatial distribution of polynya and lead occurrences is also visible in our here derived TIT frequencies (e.g. eastern exit Vilkitzky Strait, Hanna Shoal / northern Chukchi Shelf, northern ESS).

In Fig. 5 and Fig. 6, the interannual variability of the average POLA (in km^2) and accumulated IP (in km^3) are presented for all examined polynya regions, respectively. In both figures, the difference between the beginning (November to December) and end (January to March) of the freezing (winter) period is additionally highlighted. Concerning POLA, it shows that the largest average wintertime extents are found in the NOW and KAR areas. The study of Preußer et al. (2015a) demonstrated that these large POLA values in the NOW-region are part of a long-term increase of average polynya extents between 1978 and 2015. As

The Cryosphere Discuss., doi:10.5194/tc-2016-133, 2016
Manuscript under review for journal The Cryosphere
Published: 21 July 2016

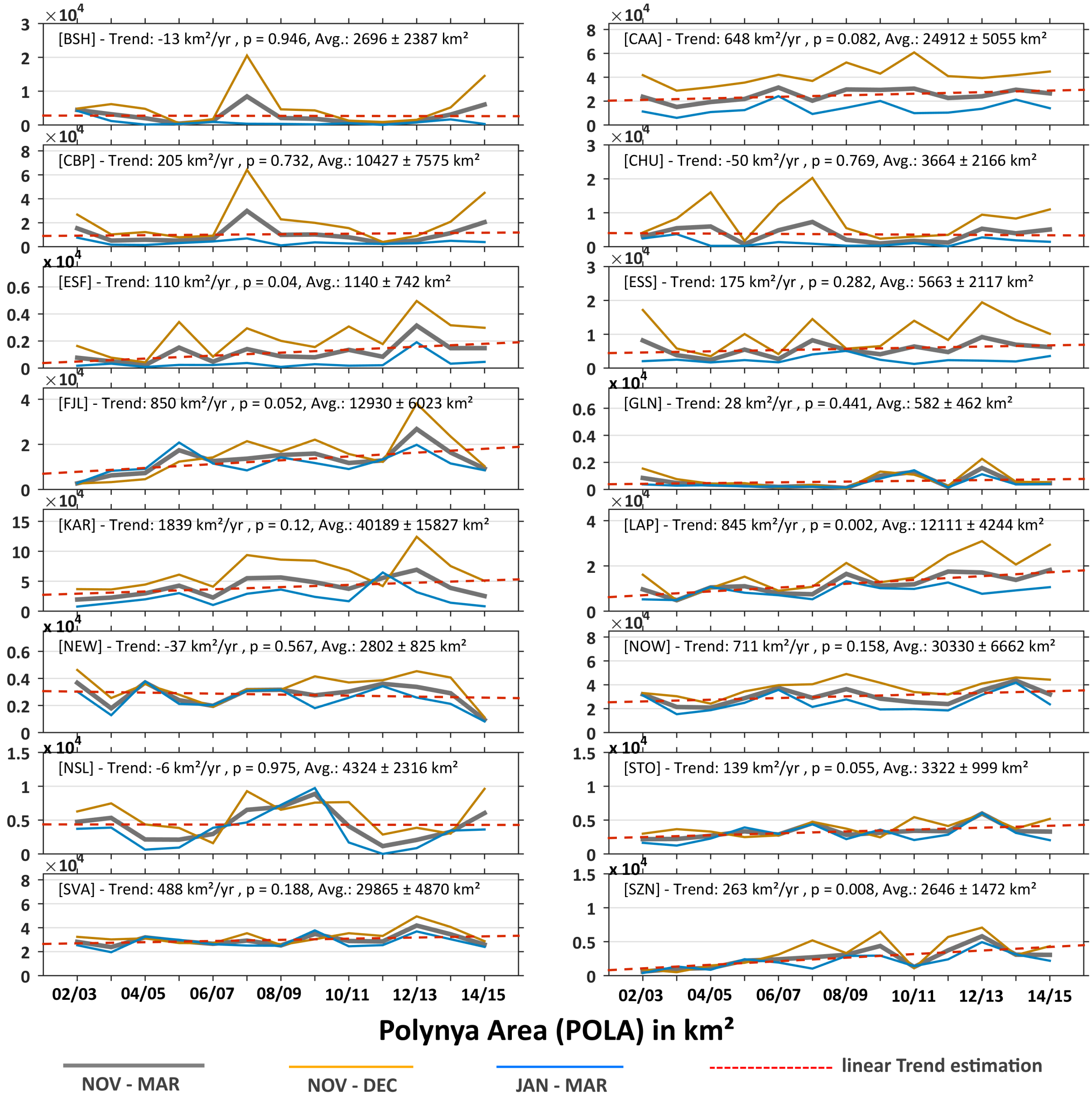

Figure 5. Regional time series of the annual average polynya area (POLA; TIT ≤ 0.2 m) in km^2 for 2002/2003 to 2014/2015, together with a seasonal comparison (November to December vs. January to March) and a linear trend estimation. The estimated linear trend (in km^2/yr), its p-value and the interannual average POLA (in km^2) are additionally listed in each sub-panel. Please note the varying scale on each y-axis.

The Cryosphere Discuss., doi:10.5194/tc-2016-133, 2016
Manuscript under review for journal The Cryosphere
Published: 21 July 2016

The Cryosphere Discussions

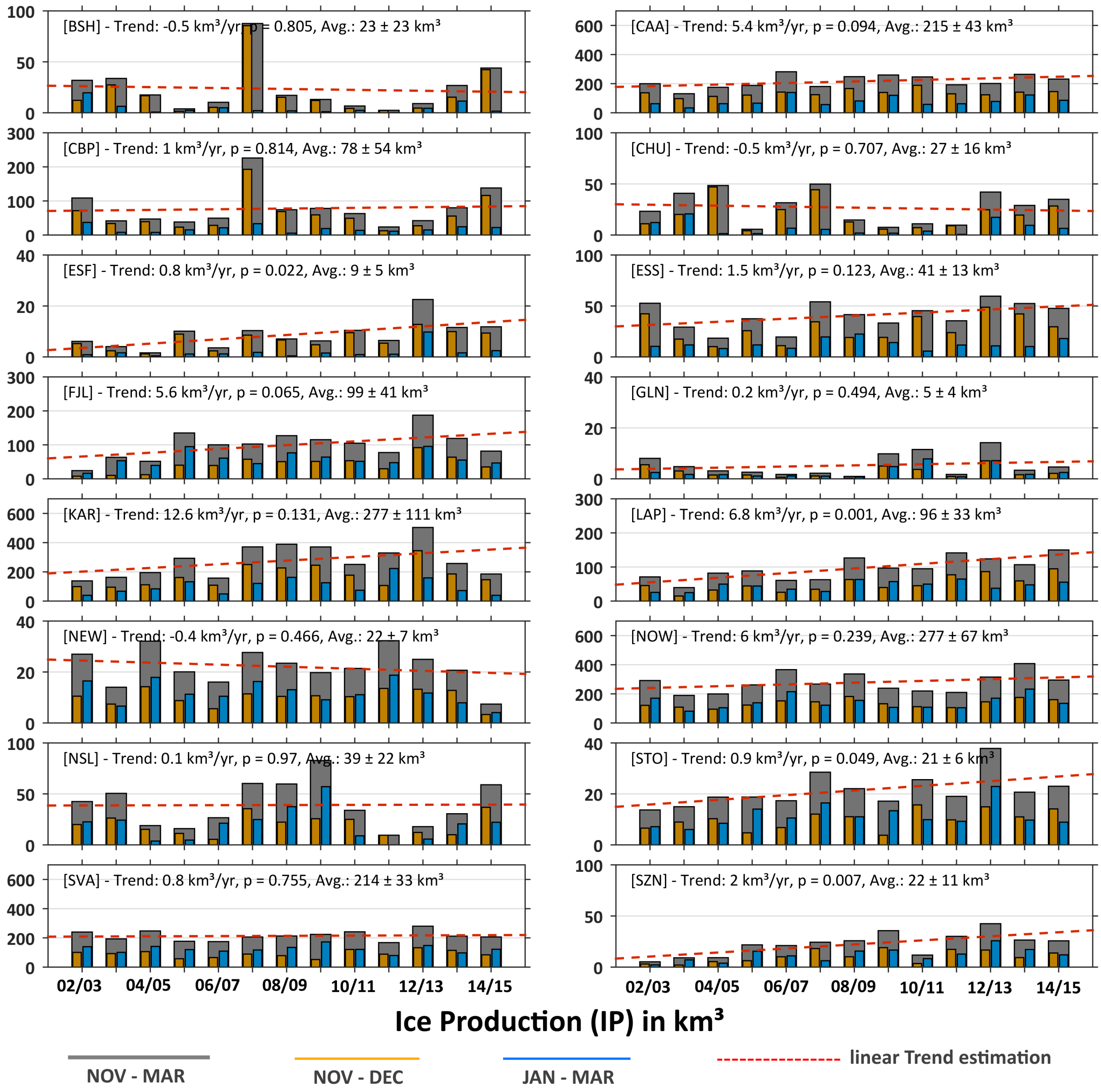

Figure 6. Regional time series of the annually accumulated ice production (IP) in km^3 for 2002/2003 to 2014/2015, together with a seasonal comparison (November to December vs. January to March) and a linear trend estimation. The estimated linear trend (in km^3/yr), its p-value and the interannual average IP (in km^3) are additionally listed in each sub-panel. Please note the varying scale on each y-axis.

The Cryosphere Discuss., doi:10.5194/tc-2016-133, 2016
Manuscript under review for journal The Cryosphere
Published: 21 July 2016

mentioned above, Kern (2008) presented POLA values for the Kara Sea. His retrievals are based on approximately the same reference area (Fig. 1), which allows for a fair comparison to the here presented numbers. It shows that the average POLA in the late freezing season reveals similar magnitudes in recent years. During the period from 1979 and 2004, the average POLA (in Kern (2008): January to April) ranged between 1 to 5 x 10^4 km^2 (except for 1995: around 6 x 10^4 km^2), which is close to the range of our here presented results for January to March (Fig.5). Although the estimated positive trend in POLA remains non-significant for the Kara Sea as in Kern (2008), the magnitude of the trend in the late freezing period (January to March; around 9000 km^2/decade) seems to have increased from 2400 km^2/decade (Kern, 2008) to around 9000 km^2/decade over the last 13 years. The interannual variability in all regions is generally pronounced, but increases for smaller polynyas / thin-ice regions such as the NSL, NEW and ESS. Concerning seasonal differences, it appears that some regions (e.g. NEW, GLN, LAP, SZN) have the tendency towards larger thin-ice areas during the freeze-up period since approximately 2006/2007 to 2007/2008. About 8 to 10 polynya regions show distinct positive trends of up to 18,390 km^2 per decade (KAR), with only the LAP, ESF and SZN regions being significant with $p \leq 0.05$. Interestingly, sub-regions located in proximity of the Beaufort Gyre (BSH and CBP) indicate very large thin-ice areas between November and December 2007, shortly after the 2nd lowest September sea-ice extent since 1979 (approx. 4.7 million km^2; Parkinson and Comiso (2013)). This did not appear in a similar way in 2012 (record low of approx. 3.4 million km^2). A detailed investigation shows that the freeze-up in the Beaufort Sea area was much slower in 2007 and extended until mid-December, while in 2012 the same area was ice-covered by November 10. The study of Timmermans (2015) linked this significant delay in ice growth to upward mixing processes of ocean heat in the Canada Basin, originating from the release of stored solar heat input following summer 2007. This resulted in large areas with very thin ice (around 170,000 km^2) in November to December and consequently allowed for huge amounts of latent and sensible heat to be released from the ocean, leading to extraordinary high IP values in these areas (Fig. 6).

Regarding IP, many of the above described features are also visible in the regional time series of Fig. 6. Contrary to Tamura and Ohshima (2011), the majority of polynya regions shows overall positive (up to 126 km^3 per decade (KAR)) or no trends in wintertime ice production, and only three regions indicate a slight decrease over the last 13 years (BSH, CHU, NEW). A complete overview on calculated average POLA and IP values per region, together with their respective trends, is given in Table 2.

The average total ice production in Arctic polynyas sums up to 1444 $\pm$ 258 km^3 per winter. Thus, it lies in between previously determined average values of 2940 $\pm$ 373 km^3 (Tamura and Ohshima, 2011; 1992/1993 - 2007/2008) and 1178 $\pm$ 65 km^3 (Iwamoto et al., 2014; 2002/2003 - 2010/2011) per winter. We expect that the MODIS-derived quantities offer a valuable increase in both spatial and quantitative accuracy due to the use of high-resolution and gap-filled daily fields of thin-ice thicknesses. In order to assess apparent differences between our here derived data-set and the passive microwave data-set by Iwamoto et al. (2014), a more direct comparison based on identical reference areas and periods would be necessary.

A spatial overview of the average (2002/2003 to 2014/2015) accumulated ice production per winter (November to March) is presented in Fig. 7. Likewise to Fig. 4, the North Water (NOW) polynya stands out at first glance due to its high average ice production of up to 14 m per winter. However, smaller polynyas in the Canadian Arctic (around Devon Island) feature comparatively high values for ice production. Most other areas in the Arctic produce on average between 1-3 m of ice per

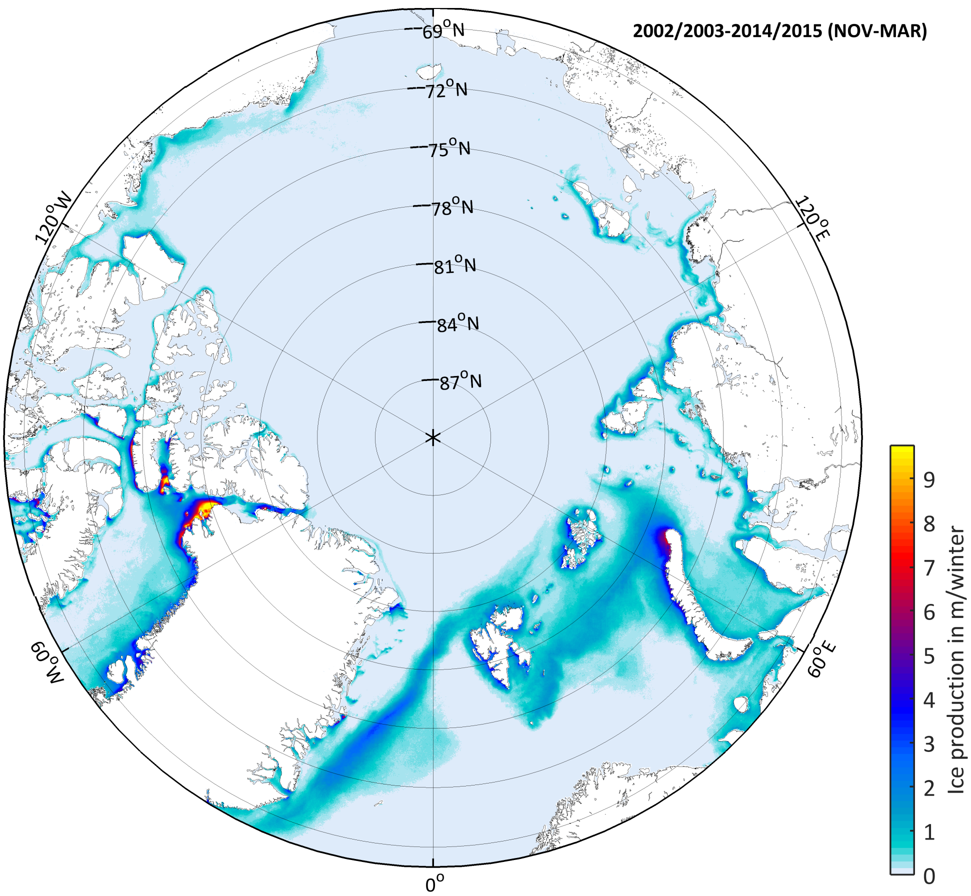

Figure 7. Average (2002/2003 to 2014/2015) accumulated ice production (m per winter) during winter (November to March) in the Arctic, north of 68° N.

winter, with a few noticeable exceptions like Franz Josef Land (about 4-5 m per winter) and some areas in the Kara Sea (1-4 m per winter). While the core areas of high ice production show a high resemblance to Iwamoto et al. (2014) with marginal differences in absolute numbers, MODIS is capable to provide enhanced spatial detail. This is especially valuable concerning the narrow thin-ice areas along the coast and fast-ice edges in the eastern part of the Arctic (Kara Sea, Laptev Sea, East Siberian Sea), as these areas are not resolved by the coarse-resolution passive microwave data (6.25 km; Iwamoto et al., 2014). This striking advantage is also reflected in the comparatively narrow fjords and bays/sounds around Greenland and the Canadian Archipelago, where a high ice production of up to 3 meters per winter is found.

Spatial trends between the winter seasons 2002/2003 and 2014/2015 can be calculated by applying a linear regression on the annual accumulated IP per pixel. The resulting map is shown in Fig. 8 (a). Besides many interesting small-scale patterns, two main conclusions can be drawn from this spatial overview: (1) While the trends identified in the western Arctic show no consistent pattern, large areas of the eastern Arctic are characterized by significant (compare Fig. 8 (b)) positive trends that

The Cryosphere Discuss., doi:10.5194/tc-2016-133, 2016
Manuscript under review for journal The Cryosphere
Published: 21 July 2016

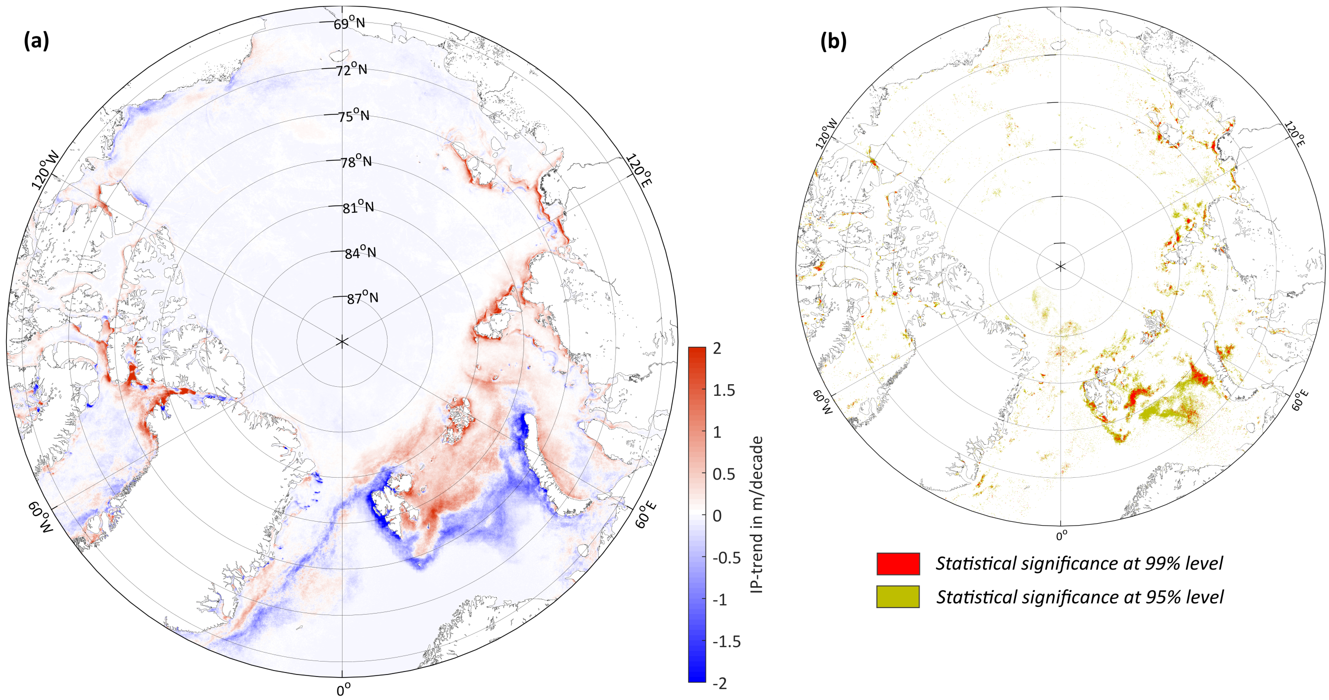

Figure 8. (a) Decadal trends (m per decade) of wintertime (November to March) ice production in the Arctic, north of 68° N. Trends are calculated by applying a linear regression on the annual accumulated IP per pixel for the period 2002/2003 to 2014/2015. Areas with statistical significance at the 95% (dark yellow) and 99% (red) level are depicted in sub-panel (b).

can exceed 2 meters per decade and (2) the structure of negative / positive spatial trends along the Siberian coast suggests a tendency towards a diminishing fast-ice extent over the recent 13 years. We suppose that this characteristic pattern of opposing trends and the 'retreating-behavior' of fast ice could be connected to a shortened freezing period (Markus et al., 2009; Stroeve et al., 2014) in recent years, resulting from a complex mixture/interplay of steadily increasing (2m-) air temperatures, distinct large-scale atmospheric patterns (e.g. Rigor et al., 2002) and the overall downward trend of total sea-ice extent and volume in the Arctic. As being one of the main regions with highly pronounced and significant positive trends in both POLA and IP, the following section will take a closer look on polynya dynamics in the Laptev Sea.

4.2 Regional focus - Laptev Sea

One main advantage of the high-resolution MODIS data is the ability to perform detailed investigations on a regional scale across the Arctic. The grid spacing of 2 km allows for the detection of relatively fine and delineated polynya structures and for more accurate statements about areas of high ice production, as it was previously possible.

The Laptev Sea was previously described as a key region to investigate climatic changes in the Arctic shelf seas (ACIA, 2005), as it is one of the major source area for sea ice export into the Transpolar Drift system (Dethleff et al., 1998). As can

The Cryosphere Discuss., doi:10.5194/tc-2016-133, 2016
Manuscript under review for journal The Cryosphere
Published: 21 July 2016

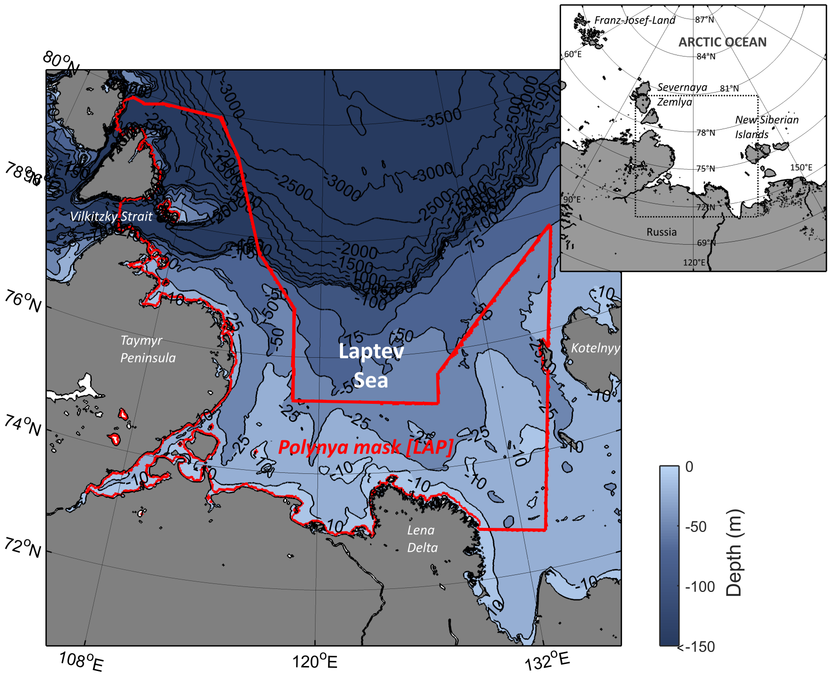

Figure 9. The geographical location of the Laptev Sea in the eastern Arctic. The applied polynya mask is marked in red, enclosing the locations of typical polynya formation along the coast and fast-ice edges. Bathymetric data by Jakobsson et al. (2012) (IBCAO v3.0).

be seen in Fig. 9, the Laptev Sea is located between the Severnaya Zemlya at the western boundary, the Lena Delta at the southern edge and the New Siberian Islands, which serve as the boundary in the East (approximately 70-80°N, 100-140°E). The water-mass composition in the Laptev Sea is temporarily quite variable, as there is a huge freshwater inflow during the summer and autumn period (around 750 km^3 per year; Rigor and Colony (1997)) and strong ice-formation accompanied with brine rejection in polynyas during winter (Bauch et al., 2012). These processes significantly alter the stratification of the upper ocean layers as well as the salinity levels in the annual cycle. These and other recurring features of the sea ice and ocean environments have recently been illustrated and updated by Janout et al. (2016).

During the freezing period (roughly October to June), fast ice forms along the coastlines of the Laptev Sea, which usually reaches its maximum areal extent by April. For drifting sea ice, the fast ice edge forms an advanced coast line, with heavy ridging occurring along this edge during onshore wind events (Rigor and Colony, 1997). The combination of this fast-ice edge and off-shore components of the mean wind-patterns enable the formation of several flaw-lead polynyas across the Laptev Sea which can reach widths of up to 200 km (Bareiss and Görgen, 2005; Martin and Cavalieri, 1989; Ernsdorf et al., 2011; Adams et al., 2013).

When comparing previous studies dealing with ice production rates in the Laptev Sea (Dethleff et al., 1998; Winsor and Björk, 2000; Dmitrenko et al., 2009; Willmes et al., 2011; Tamura and Ohshima, 2011; Bauer et al., 2013; Iwamoto et al., 2014; Gutjahr et al., 2016), it gets clear that there are large differences depending on the applied methods and various different

The Cryosphere Discuss., doi:10.5194/tc-2016-133, 2016
Manuscript under review for journal The Cryosphere
Published: 21 July 2016

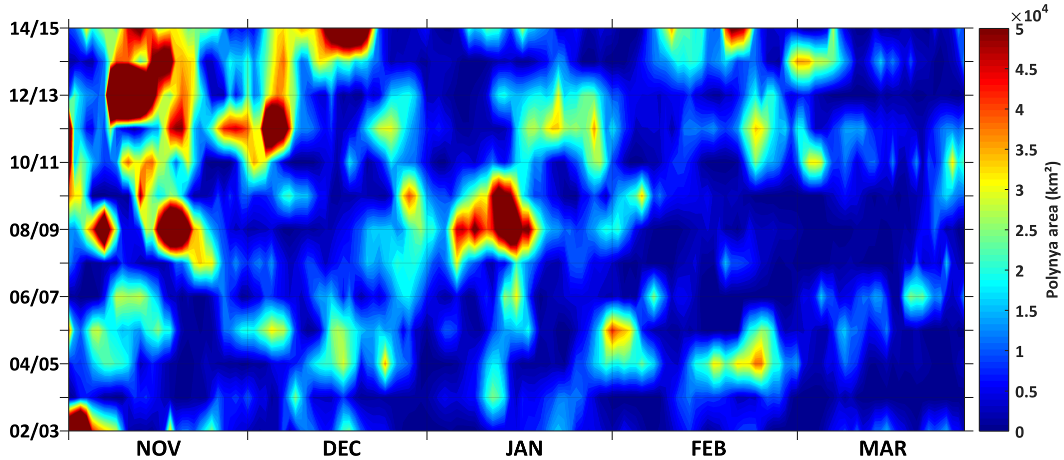

Figure 10. Hovmoeller plot of the daily polynya area (TIT ≤ 0.2 m) in the Laptev Sea region. Values are calculated within the margins of the applied polynya mask (Fig. 1) and saturated at a level of 5 x 10^4 km^2 for a better discrimination of lower values.

data-sets. In these studies, values for the accumulated ice production during an average winter season ('extended' winter-period from November to April) are ranging between 55 km^3 (Willmes et al., 2011) for an approach using microwave and thermal infrared remote sensing data in combination with atmospheric reanalysis data, and 258 km^3 (Dethleff et al., 1998), who used a simple relationship between wind direction/speed and polynya area. Estimated average values (September to May) from Tamura and Ohshima (2011) (152 km^3) and Iwamoto et al. (2014) (77 km^3) range in between. Although derived for different time periods and slightly varying reference areas, these large discrepancies highlight the relevance of applying improved and high-resolution approaches to quantify sea-ice production.

In order to give an overview on the long-term development of thin-ice areas (TIT ≤ 0.2 m) in the Laptev Sea, the daily POLA is presented in Fig. 10. It is evident that the largest POLA values appear on average in November and more recently also in December. A tendency towards an increased duration of these polynya-events can be observed. In the winter-seasons 2008/2009 and 2009/2010, large POLA exceeding 50000 km^2 are also observed in January and another major polynya event can be noted for mid-February 2015. A pronounced seasonal variation is visible for about half of the 13-year record, while some other years (prior to 2010/2011) show only weak polynya activity in February and March.

Fig. 11 shows an annual comparison (2002/2003 to 2014/2015) of accumulated ice production (in m per winter) for the Laptev Sea. The highest ice-production rates of sometimes more than 4 m per winter occur predominantly in proximity of the Taymyr Peninsula and Severnaya Zemlya (western Laptev Sea), as well as along the southern fast-ice edge. However, ice production in the eastern Laptev Sea (west and north of the New Siberian Islands) shows a greater inter-annual variability. Furthermore, it is striking that the position of the fast-ice edge in Fig. 11 is highly variable over the 13-yr record (as noted in Sect. 3.1, Fig. 8 (a)). Another interesting observation can be made in the Vilkitzky Strait, which is located in the western Laptev Sea south of Severnaya Zemlya (Fig. 9). The distribution of thin-ice areas contributing significantly to the total sea-

The Cryosphere Discuss., doi:10.5194/tc-2016-133, 2016
Manuscript under review for journal The Cryosphere
Published: 21 July 2016

The Cryosphere
Discussions
Open Access

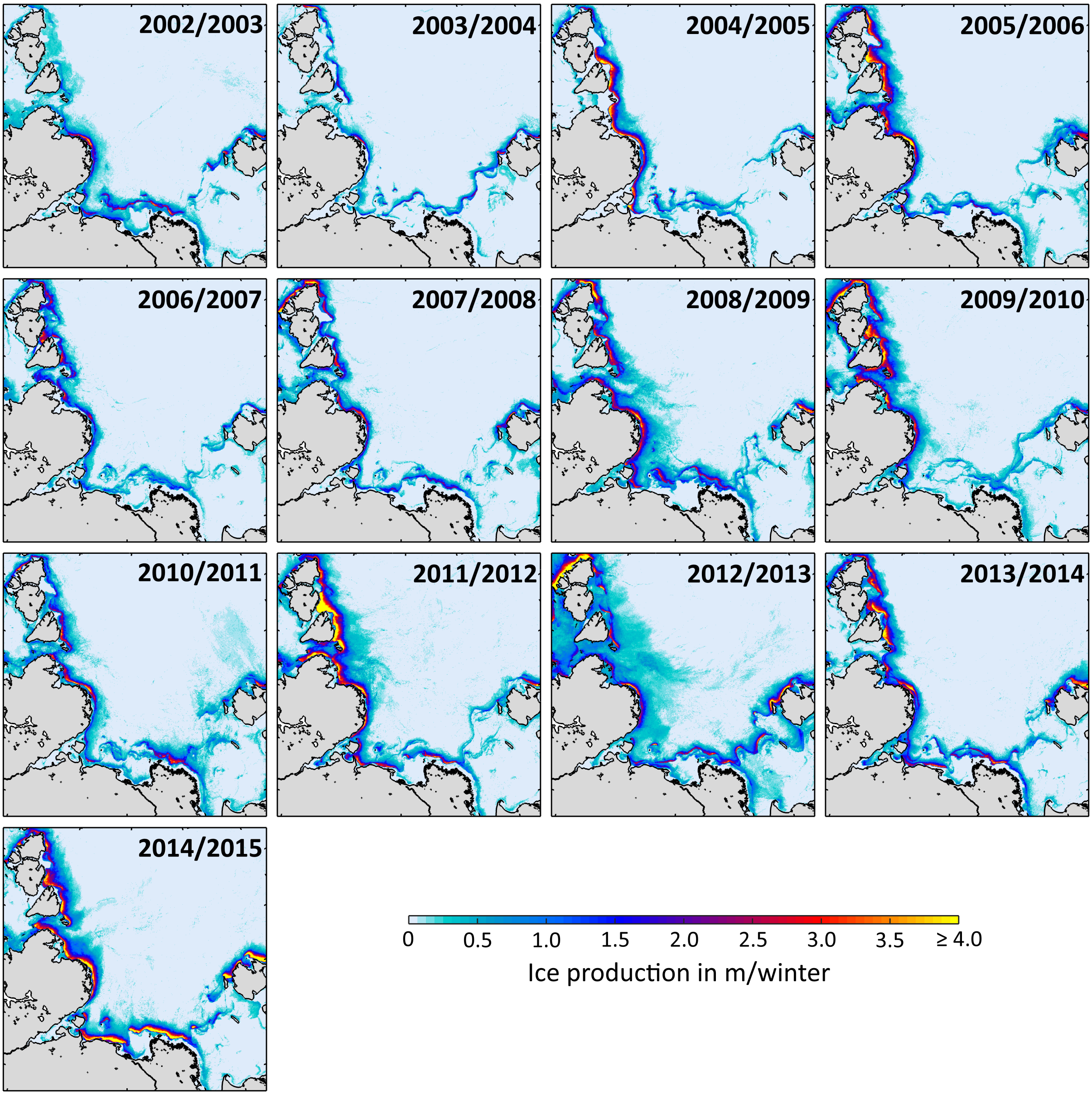

Figure 11. Overview of wintertime (November to March) accumulated ice production (m per winter) in the Laptev Sea region between 2002/2003 and 2014/2015.

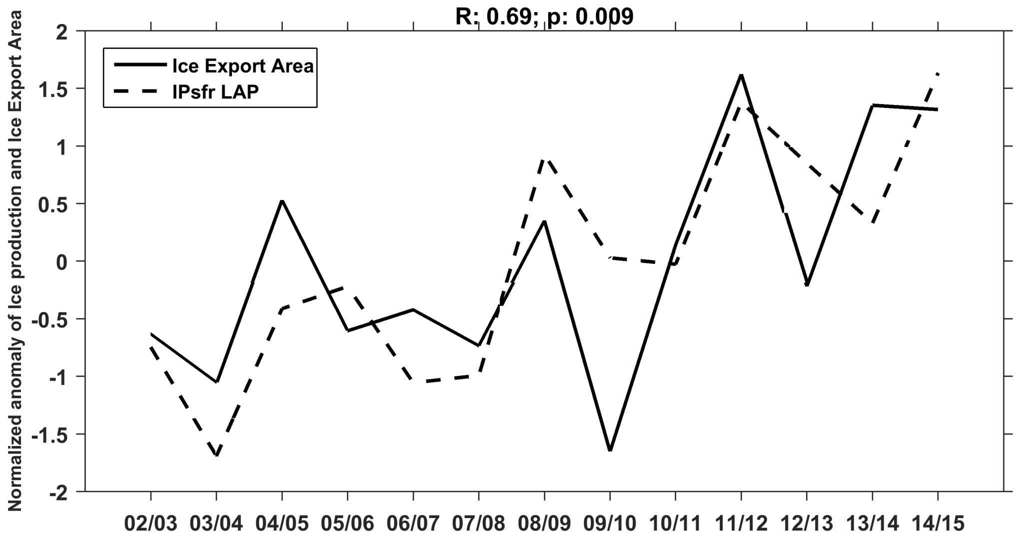

Figure 12. Normalized anomalies of accumulated wintertime ice production (IP of the present study; dashed line) and accumulated Ice Area Export (IAE; solid line) for winter seasons 2002/2003 to 2014/2015. IAE data is based on an updated time series by Krumpen et al. (2013).

ice production in that area seems to shift westwards towards the Kara Sea in several years (2005/2006 to 2012/2013 and 2014/2015). In some cases, the shape of these areas resembles an arch-type/ice-bridge pattern/mechanism, a feature that is commonly appearing e.g. in Nares Strait between Ellesmere Island and Greenland (Williams et al., 2007).

Krumpen et al. (2013) discovered that most of the ice being incorporated in the Transpolar Drift originates from the western and central part of the Laptev Sea. Further, it was indicated that the contribution from polynyas, while being generally small, is limited to events in proximity of the Laptev Sea boundaries. As noted before, the north-western Laptev Sea shows by far the largest contribution to the total wintertime ice production in the Laptev Sea polynyas, which implies a potential significant influence on the interannual variability of the ice export during winter. In order to check this hypothesis, we compare annual accumulated IP values to independently derived ice-area export (IAE) values (both presented as anomalies and normalized with their standard deviation) in Fig. 12 for 2002/2003 to 2014/2015. IAE values are taken from the updated time series of Krumpen et al. (2013). Likewise to a high agreement between polynya area and across-boundary ice export (Krumpen et al., 2013), there is also a significant correlation between calculated ice production and the areal ice export (r = 0.69).

The spatial overview of annual ice production (Fig. 11) is supplemented by the previously shown time series of the average wintertime POLA and accumulated IP per winter (Fig. 5 and Fig. 6, respectively). Both time series of POLA and IP in the Laptev Sea show an overall positive trend (significant with $p \leq 0.01$), which can for the most part be traced back to larger thin-ice areas during the freeze-up period in November and December (as decribed above; Fig. 10). The average ice production from November to March in the Laptev Sea is estimated with about $96 \pm 33\ \mathrm{km}^3$ (2002/2003 - 2014/2015), with a positive trend of 6.8 km^3 per year. Compared to other Arctic polynyas (compare Tab. 2), this corresponds to a share of about 7% of the total ice production in polynya regions.

The Cryosphere Discuss., doi:10.5194/tc-2016-133, 2016
Manuscript under review for journal The Cryosphere
Published: 21 July 2016

As the relative strength of the Transpolar Drift is dependent on atmospheric dynamics, it has previously been linked to atmospheric indices like the Arctic Oscillation (AO) Index (Rigor and Wallace, 2004). For the period from 1982 to 2009, the study by Kwok et al. (2013) presented indicators for a net-strengthening of both the Transpolar Drift and the Beaufort Gyre as well as a general increase of the Arctic ice drift-speed. The latter is presumably connected to a decreasing fraction of multi-year (MY) ice and a more fragile, thus mobile, sea-ice cover with potential implications for polynya and lead dynamics not only in the eastern Arctic. According to Rigor et al. (2002), a positive winter AO promotes both an increased ice transport out of the Arctic Ocean through Fram Strait and an increased ice transport away from the Siberian coastal areas, thereby leaving open water and thin ice that foster new ice formation. Hence, positive trends in both POLA and IP not only fit well to the previously estimated positive trend in IP from Iwamoto et al. (2014) but also to the positive trend of 0.85 x 10^5 km^2 per decade in the Laptev Sea ice area flux (Krumpen et al., 2013). Other linkages and dependencies with the Arctic sea-ice extent in September (annual minimum), the length of the freezing period and further connections to large-scale atmospheric circulation patterns are very likely and have been proposed by various previous studies (e.g. Alexandrov et al. (2000); Deser et al. (2000); Rigor et al. (2002); Willmes et al. (2011); Krumpen et al. (2013), but do require more detailed investigations that go beyond the scope of this paper.

5 Conclusions

In the present study we analyzed circumpolar polynya dynamics and ice production in the Arctic based on high-resolution MODIS thermal infrared imagery and atmospheric reanalysis from the ERA-Interim data set. Pan-Arctic and (quasi-) daily thin-ice thickness distributions were calculated using a 1D-energy balance model for the period from 2002/2003 to 2014/2015 (November to March). After applying a necessary and well-working gap-filling approach to compensate for cloud and data gaps, the thermodynamic ice production was derived by assuming that all heat loss at the ice surface contributes to the growth of sea ice. We presented results for 16 prominent polynya regions, whereby the a strong focus was set on the Laptev Sea region in the eastern Arctic. Despite existing limitations originating from the use of thermal infrared remote sensing data during winter, we think that this new data set of 13 consecutive winter seasons is a huge step forward for an accurate characterization of Arctic polynya dynamics and the seasonal sea-ice budget in general. Our main findings and conclusions are the following:

(1) The use of high-resolution MODIS data increases the capability to resolve small scale (> 2km) thin-ice features such as narrow polynyas and leads, which therefore contribute to our ice production estimates. This represents an advantage compared to other (passive microwave) data sets.

(2) The average wintertime accumulated ice production in all 16 polynya regions is estimated with about 1444 ± 258 km^3. The largest contributions originate from the Kara Sea region and the North Water polynya (both 19%) as well as scattered smaller polynyas in the (eastern) Canadian Arctic Archipelago (all combined around 15%). Compared to the most recent study on ice production in Arctic polynyas by Iwamoto et al. (2014), our estimate on the average total ice production is about 22% larger, although differences in the regarded time frame, reference areas and applied satellite sensors certainly contribute to this discrepancy.

The Cryosphere Discuss., doi:10.5194/tc-2016-133, 2016
Manuscript under review for journal The Cryosphere
Published: 21 July 2016

(3) Positive trends in ice production can be detected for several regions of the eastern Arctic (most significant in the Laptev Sea region with an increase of 6.8 km^3/yr and the North Water polynya, while other polynyas in the western Arctic show a more pronounced interannual variability with even slightly negative trends in the Beaufort and Chukchi Sea as well as the North-East Water polynya. These regionally different trends are considered to be caused by changes in the overall sea-ice mobility (i.e. sea-ice drift), temporal shifts in the length of the ice growth-/melt-seasons and distinct large-scale atmospheric set-ups that promoted an increased ice export and enhanced ice production in the Siberian shelf regions.

(4) The Laptev Sea region was chosen as a special focus in our study as it is one of the core areas for ice production in the Arctic with a distinct connection to Transpolar Drift characteristics and showing a strong positive trend. Ice production in the Laptev Sea was mapped with enhanced spatial detail, which is especially valuable in this region with narrow and elongated flaw leads close to the fast-ice edge. Our results showed that polynyas in the Laptev Sea contribute with at least 7% to the total potential sea-ice production in Arctic polynyas. While the interannual variability in terms of location and extent seems to be rather high, the positive trends in both POLA and IP time series fit well to results from previous studies in the Laptev Sea, which described increasing atmosphere- and ocean-temperatures (Boisvert and Stroeve, 2015), a significant lengthening of the melt season (Stroeve et al., 2014), a shortened fast-ice duration (Selyuzhenok et al., 2015) and increasing sea-ice area export (Krumpen et al., 2013), among other changes during the spring and summer period (Janout et al., 2016). Future comparisons with newly derived volume-flux estimates in the Transpolar Drift (Krumpen et al., 2016) certainly promise further insights on the absolute contribution of polynyas to the volume ice export out of the Laptev Sea and adjacent seas.

(5) The qualitative comparison to the MODIS-derived lead product by Willmes and Heinemann (2016) reveals a shortcoming of the here applied SFR-algorithm, as it is not entirely possible to adequately reconstruct leads with a low spatial and temporal persistence. A thoughtful combination of both concepts is therefore a goal worth to achieve for future/continuing investigations on thin-ice regions in the polar regions using thermal infrared data from MODIS or other comparable satellite sensors, allowing for estimates of IP by leads also for the central Arctic ocean.

Author contributions. Andreas Preußer carried out the complete analysis and drafted the manuscript. Sascha Willmes and Stephan Paul supported the satellite data analysis and further processing. All co-authors contributed to the writing of the manuscript. The final draft of the manuscript was revised and approved by all of the authors.

Acknowledgements. The authors want to thank the National Snow and Ice Data Center (NSIDC) as well as the European Center for Medium-Range Weather Forecasts (ECMWF) for providing the MODIS Sea Ice product (ftp://n5eil01u.ecs.nsidc.org/SAN/) and the ERA-Interim atmospheric reanalysis data. The provision of the ice area export data set by Dr. Thomas Krumpen (Alfred Wegener Institute, Bremerhaven, Germany) as well as related discussions are highly acknowledged. This work was funded by the Federal Ministry of Education and Research (Bundesministerium für Bildung und Forschung - BMBF) under Grant 03G0833D.

References

ACIA: Arctic Climate Impact Assessment. ACIA Overview report., Cambridge University Press, 2005.

Ackerman, S., Frey, R., Strabala, K., Liu, Y., Gumley, L., Baum, B., and Menzel, P.: Discriminating clear-sky from cloud with MODIS algorithm theoretical basis document (MOD35) Version 6.1, Tech. rep., MODIS Cloud Mask Team, Cooperative Institute for Meteorological Satellite Studies, University of Wisconsin, 2010.

Adams, S., Willmes, S., Schroeder, D., Heinemann, G., Bauer, M., and Krumpen, T.: Improvement and sensitivity analysis of thermal thin-ice retrievals, IEEE Transactions on Geoscience and Remote Sensing, 51, 3306–3318, doi:10.1109/tgrs.2012.2219539, 2013.

Alexandrov, V. Y., Martin, T., Kolatschek, J., Eicken, H., Kreyscher, M., and Makshtas, A. P.: Sea ice circulation in the Laptev Sea and ice export to the Arctic Ocean: Results from satellite remote sensing and numerical modeling, Journal of Geophysical Research, 105, 17 143–17 159, 2000.

Barber, D. G. and Massom, R. A.: The Role of Sea Ice in Arctic and Antarctic Polynyas, in: Polynyas - Windows to the World, edited by Smith, W. O. and Barber, D. G., chap. The Role of Sea Ice in Arctic and Antarctic Polynyas, pp. 1–54, Elsevier Oceanography Series, doi:10.1016/s0422-9894(06)74001-6, 2007.

Bareiss, J. and Görgen, K.: Spatial and temporal variability of sea ice in the Laptev Sea: Analyses and review of satellite passive-microwave data and model results, 1979 to 2002, Global and Planetary Change, 48, 28–54, 2005.

Bauch, D., Hlemann, J. A., Dmitrenko, I. A., Janout, M. A., Nikulina, A., Kirillov, S. A., Krumpen, T., Kassens, H., and Timokhov, L.: Impact of Siberian coastal polynyas on shelf-derived Arctic Ocean halocline waters, J. Geophys. Res., 117, n/a–n/a, doi:10.1029/2011jc007282, http://dx.doi.org/10.1029/2011JC007282, 2012.

Bauer, M., Schröder, D., Heinemann, G., Willmes, S., and Ebner, L.: Quantifying polynya ice production in the Laptev Sea with the COSMO model, Polar Research, 32, doi:10.3402/polar.v32i0.20922, http://www.polarresearch.net/index.php/polar/article/view/20922, 2013.

Boisvert, L. N. and Stroeve, J. C.: The Arctic is becoming warmer and wetter as revealed by the Atmospheric Infrared Sounder, Geophysical Research Letters, 42, 4439–4446, doi:10.1002/2015GL063775, http://dx.doi.org/10.1002/2015GL063775, 2015GL063775, 2015.

Dee, D. P., Uppala, S. M., Simmons, A. J., Berrisford, P., Poli, P., Kobayashi, S., Andrae, U., Balmaseda, M. A., Balsamo, G., Bauer, P., Bechtold, P., Beljaars, A. C. M., van de Berg, L., Bidlot, J., Bormann, N., Delsol, C., Dragani, R., Fuentes, M., Geer, A. J., Haimberger, L., Healy, S. B., Hersbach, H., Hólm, E. V., Isaksen, L., Kållberg, P., Köhler, M., Matricardi, M., McNally, A. P., Monge-Sanz, B. M., Morcrette, J.-J., Park, B.-K., Peubey, C., de Rosnay, P., Tavolato, C., Thépaut, J.-N., and Vitart, F.: The ERA-Interim reanalysis: configuration and performance of the data assimilation system, Quarterly Journal of the Royal Meteorological Society, 137, 553–597, doi:10.1002/qj.828, 2011.

Deser, C., Walsh, J. E., and Timlin, M. S.: Arctic sea ice variability in the context of recent atmospheric circulation trends, Journal of Climate, 13, 617–633, 2000.

Dethleff, D., Loewe, P., and Kleine, E.: The Laptev Sea flaw leaddetailed investigation on ice formation and export during 1991/1992 winter season, Cold Regions Science and Technology, 27, 225–243, 1998.

Dmitrenko, I. A., Kirillov, S. A., Tremblay, L. B., Bauch, D., and Willmes, S.: Sea-ice production over the Laptev Sea shelf inferred from historical summer-to-winter hydrographic observations of 1960s–1990s, Geophysical Research Letters, 36, 2009.

Drucker, R., Martin, S., and Moritz, R.: Observations of ice thickness and frazil ice in the St. Lawrence Island polynya from satellite imagery, upward looking sonar, and salinity/temperature moorings, J. Geophys. Res., 108, 3149, doi:10.1029/2001jc001213, 2003.

The Cryosphere Discuss., doi:10.5194/tc-2016-133, 2016
Manuscript under review for journal The Cryosphere
Published: 21 July 2016

Ebner, L., Schröder, D., and Heinemann, G.: Impact of Laptev Sea flaw polynyas on the atmospheric boundary layer and ice production using idealized mesoscale simulations, Polar Research, 30 (7210), 16, doi:10.3402/polar.v30i0.7210, 2011.

Ernsdorf, T., Schrder, D., Adams, S., Heinemann, G., Timmermann, R., and Danilov, S.: Impact of atmospheric forcing data on simulations of the Laptev Sea polynya dynamics using the sea-ice ocean model FESOM, J. Geophys. Res., 116, doi:10.1029/2010jc006725, http://dx.doi.org/10.1029/2010JC006725, 2011.

Gutjahr, O., Heinemann, G., Preußer, A., Willmes, S., and Drüe, C.: Sensitivity of ice production estimates in Laptev Sea polynyas to the parameterization of subgrid-scale sea-ice inhomogeneities in COSMO-CLM, The Cryosphere Discussions, 2016, 1–34, doi:10.5194/tc-2016-83, http://www.the-cryosphere-discuss.net/tc-2016-83/, 2016.

Haid, V., Timmermann, R., Ebner, L., and Heinemann, G.: Atmospheric forcing of coastal polynyas in the south-western Weddell Sea, Antarctic Science, 27, 388–402, doi:10.1017/s0954102014000893, http://dx.doi.org/10.1017/S0954102014000893, 2015.

Hall, D., Key, J., Casey, K., Riggs, G., and Cavalieri, D.: Sea ice surface temperature product from MODIS, Geoscience and Remote Sensing, IEEE Transactions on, 42, 1076 – 1087, doi:10.1109/tgrs.2004.825587, 2004.

Hannah, C. G., Dupont, F., and Dunphy, M.: Polynyas and tidal currents in the Canadian Arctic Archipelago, Arctic, pp. 83–95, 2009.

Hirano, D., Fukamachi, Y., Watanabe, E., Ohshima, K. I., Iwamoto, K., Mahoney, A. R., Eicken, H., Simizu, D., and Tamura, T.: A wind-driven, hybrid latent and sensible heat coastal polynya off Barrow, Alaska, Journal of Geophysical Research: Oceans, doi:10.1002/2015JC011318, 2016.

Iwamoto, K., Ohshima, K. I., and Tamura, T.: Improved mapping of sea ice production in the Arctic Ocean using AMSR-E thin ice thickness algorithm, Journal of Geophysical Research: Oceans, 119, 3574–3594, doi:10.1002/2013jc009749, http://onlinelibrary.wiley.com/doi/10.1002/2013JC009749/abstract, 2014.

Jakobsson, M., Mayer, L., Coakley, B., Dowdeswell, J. A., Forbes, S., Fridman, B., Hodnesdal, H., Noormets, R., Pedersen, R., Rebesco, M., Schenke, H. W., Zarayskaya, Y., Accettella, D., Armstrong, A., Anderson, R. M., Bienhoff, P., Camerlenghi, A., Church, I., Edwards, M., Gardner, J. V., Hall, J. K., Hell, B., Hestvik, O., Kristoffersen, Y., Marcussen, C., Mohammad, R., Mosher, D., Nghiem, S. V., Pedrosa, M. T., Travaglini, P. G., and Weatherall, P.: The international bathymetric chart of the Arctic Ocean (IBCAO) version 3.0, Geophysical Research Letters, 39, doi:10.1029/2012gl052219, 2012.

Janout, M., Hölemann, J., Juhls, B., Krumpen, T., Rabe, B., Bauch, D., Wegner, C., Kassens, H., and Timokhov, L.: Episodic warming of near-bottom waters under the Arctic sea ice on the central Laptev Sea shelf, Geophysical Research Letters, 43, 264–272, doi:10.1002/2015GL066565, http://dx.doi.org/10.1002/2015GL066565, 2015GL066565, 2016.

Kern, S.: Polynya area in the Kara Sea, Arctic, obtained with microwave radiometry for 1979–2003, Geoscience and Remote Sensing Letters, IEEE, 5, 171–175, 2008.

Krumpen, T., Janout, M., Hodges, K., Gerdes, R., Girard-Ardhuin, F., Hölemann, J., and Willmes, S.: Variability and trends in Laptev Sea ice outflow between 1992–2011, The Cryosphere, 7, 1–15, 2013.

Krumpen, T., Gerdes, R., Haas, C., Hendricks, S., Herber, A., Selyuzhenok, V., Smedsrud, L., and Spreen, G.: Recent summer sea ice thickness surveys in Fram Strait and associated ice volume fluxes, The Cryosphere, 10, 523–534, doi:10.5194/tc-10-523-2016, http://www.the-cryosphere.net/10/523/2016/, 2016.

Kwok, R., Spreen, G., and Pang, S.: Arctic sea ice circulation and drift speed: Decadal trends and ocean currents, Journal of Geophysical Research: Oceans, 118, 2408–2425, 2013.

Liu, Y. and Key, J. R.: Less winter cloud aids summer 2013 Arctic sea ice return from 2012 minimum, Environmental Research Letters, 9, 044 002, doi:10.1088/1748-9326/9/4/044002, http://dx.doi.org/10.1088/1748-9326/9/4/044002, 2014.

Markus, T., Stroeve, J. C., and Miller, J.: Recent changes in Arctic sea ice melt onset, freezeup, and melt season length, J. Geophys. Res., 114, doi:10.1029/2009jc005436, http://dx.doi.org/10.1029/2009JC005436, 2009.

Martin, S.: Frazil ice in rivers and oceans, Annual Review of Fluid Mechanics, 13, 379–397, doi:10.1146/annurev.fl.13.010181.002115, 1981.

Martin, S. and Cavalieri, D. J.: Contributions of the Siberian shelf polynyas to the Arctic Ocean intermediate and deep water, Journal of Geophysical Research: Oceans, 94, 12 725–12 738, 1989.

Melling, H., Haas, C., and Brossier, E.: Invisible polynyas: Modulation of fast ice thickness by ocean heat flux on the Canadian polar shelf, Journal of Geophysical Research, Oceans, 120, 777–795, doi:10.1002/2014jc010404, http://dx.doi.org/10.1002/2014JC010404, 2015.

Morales-Maqueda, M., Willmott, A., and Biggs, N.: Polynya dynamics: A review of observations and modeling, Reviews of Geophysics, 42, 1–37, doi:10.1029/2002rg000116, 2004.

Parkinson, C. L. and Comiso, J. C.: On the 2012 record low Arctic sea ice cover: Combined impact of preconditioning and an August storm, Geophysical Research Letters, 40, 1356–1361, 2013.

Paul, S., Willmes, S., Gutjahr, O., Preußer, A., and Heinemann, G.: Spatial Feature Reconstruction of Cloud-Covered Areas in Daily MODIS Composites, Remote Sensing, 7, 5042–5056, doi:10.3390/rs70505042, 2015a.

Paul, S., Willmes, S., and Heinemann, G.: Long-term coastal-polynya dynamics in the Southern Weddell Sea from MODIS thermal-infrared imagery, The Cryosphere, 9, 2027–2041, doi:10.5194/tc-9-2027-2015, 2015b.

Preußer, A., Heinemann, G., Willmes, S., and Paul, S.: Multi-Decadal Variability of Polynya Characteristics and Ice Production in the North Water Polynya by Means of Passive Microwave and Thermal Infrared Satellite Imagery, Remote Sensing, 7, 15 844–15 867, 2015a.

Preußer, A., Willmes, S., Heinemann, G., and Paul, S.: Thin-ice dynamics and ice production in the Storfjorden polynya for winter seasons 2002/2003-2013/2014 using MODIS thermal infrared imagery, The Cryosphere, 9, 1063–1073, doi:10.5194/tc-9-1063-2015, http://www.the-cryosphere.net/9/1063/2015/, 2015b.

Riggs, G., Hall, D., and Salomonson, V.: MODIS Sea Ice Products User Guide to Collection 5, National Snow and Ice Data Center, University of Colorado, Boulder, CO 80309-0449 USA, http://nsidc.org/data/docs/daac/modis_v5/dorothy_ice_doc.pdf, 2006.

Rigor, I. and Colony, R.: Sea-ice production and transport of pollutants in the Laptev Sea, 1979–1993, Science of the Total Environment, 202, 89–110, 1997.

Rigor, I. G. and Wallace, J. M.: Variations in the age of Arctic sea-ice and summer sea-ice extent, Geophysical Research Letters, 31, 2004.

Rigor, I. G., Wallace, J. M., and Colony, R. L.: Response of sea ice to the Arctic Oscillation, Journal of Climate, 15, 2648–2663, 2002.

Selyuzhenok, V., Krumpen, T., Mahoney, A., Janout, M., and Gerdes, R.: Seasonal and interannual variability of fast ice extent in the southeastern Laptev Sea between 1999 and 2013, Journal of Geophysical Research: Oceans, lera, 2015.

Smith, S. D., Muench, R. D., and Pease, C. H.: Polynyas and leads: An overview of physical processes and environment, Journal of Geophysical Research, 95, 9461–9479, doi:10.1029/jc095ic06p09461, 1990.

Spreen, G., Kaleschke, L., and Heygster, G.: Sea ice remote sensing using AMSR-E 89 GHz channels, Journal of Geophysical Research, 113, doi:10.1029/2005JC003384, 2008.

Steffen, K.: Warm water cells in the North Water, northern Baffin Bay during winter, Journal of Geophysical Research: Oceans, 90, 9129–9136, doi:10.1029/JC090iC05p09129, 1985.

Stroeve, J., Markus, T., Boisvert, L., Miller, J., and Barrett, A.: Changes in Arctic melt season and implications for sea ice loss, Geophysical Research Letters, 41, 1216–1225, 2014.

The Cryosphere Discuss., doi:10.5194/tc-2016-133, 2016
Manuscript under review for journal The Cryosphere
Published: 21 July 2016

Tamura, T. and Ohshima, K. I.: Mapping of sea ice production in the Arctic coastal polynyas, J. Geophys. Res., 116, C07 030, doi:10.1029/2010jc006586, 2011.

Tamura, T., Ohshima, K. I., Markus, T., Cavalieri, D. J., Nihashi, S., and Hirasawa, N.: Estimation of Thin Ice Thickness and Detection of Fast Ice from SSM/I Data in the Antarctic Ocean, J. Atmos. Oceanic Technol., 24, 1757–1772, doi:10.1175/jtech2113.1, 2007.

Tamura, T., Ohshima, K. I., and Nihashi, S.: Mapping of sea ice production for Antarctic coastal polynyas, Geophys. Res. Lett., 35, L07 606, doi:10.1029/2007gl032903, 2008.

Timco, G. and Frederking, R.: A review of sea ice density, Cold Regions Science and Technology, 24, 1–6, doi:10.1016/0165-232X(95)00007-X, 1996.

Timmermans, M.-L.: The impact of stored solar heat on Arctic sea ice growth, Geophysical Research Letters, 42, 6399–6406, 2015.

Williams, W. J., Carmack, E. C., and Ingram, R. G.: Physical Oceanography of Polynyas, in: Polynyas - Windows to the World, edited by Smith, W. O. and Barber, D. G., chap. Physical Oceanography of Polynyas, pp. 55–86, Elsevier, 2007.

Willmes, S. and Heinemann, G.: Sea-Ice Wintertime Lead Frequencies and Regional Characteristics in the Arctic, 2003–2015, Remote Sensing, 8, 4, 2016.

Willmes, S., Krumpen, T., Adams, S., Rabenstein, L., Haas, C., Hoelemann, J., Hendricks, S., and Heinemann, G.: Cross-validation of polynya monitoring methods from multisensor satellite and airborne data: a case study for the Laptev Sea, Canadian Journal of Remote Sensing, 36, S196–S210, doi:10.5589/m10-012, 2010.

Willmes, S., Adams, S., Schröder, D., and Heinemann, G.: Spatio-temporal variability of polynya dynamics and ice production in the Laptev Sea between the winters of 1979/80 and 2007/08, Polar Research, 30 (5971), 16, doi:10.3402/polar.v30i0.5971, 2011.

Winsor, P. and Björk, G.: Polynya activity in the Arctic Ocean from 1958 to 1997, Journal of Geophysical Research, 105, 8789–8803, 2000.

Yu, Y. and Lindsay, R.: Comparison of thin ice thickness distributions derived from RADARSAT Geophysical Processor System and advanced very high resolution radiometer data sets, J. Geophys. Res., 108, 3387, doi:10.1029/2002jc001319, 2003.

Yu, Y. and Rothrock, D. A.: Thin ice thickness from satellite thermal imagery, J. Geophys. Res., 101, 25 753–25 766, doi:10.1029/96jc02242, 1996.